BMC Musculoskeletal Disorders

RESEARCH

Open Access

Hepcidin knockout exacerbates hindlimb unloading-induced bone loss in mice through inhibiting osteoblastic differentiation

Xin Chen[1,2,3], Jianping Wang[1,2,3], Chenxiao Zhen[1,2,3], Gejing Zhang[1,2,3], Zhouqi Yang[1,2,3], Youjia Xu[4] and Peng Shang[2,3*]

Abstract

Background An oligopeptide hepcidin is encoded by the human HAMP gene (Hamp in mice). Its deficiency can result in iron overload, while excess may lead to iron deficiency. Hepcidin knockout mice exhibited iron accumulation in multiple tissues, accompanied by degeneration of bone microarchitecture and reduced biomechanical properties. Astronauts who are exposed to weightlessness during prolonged spaceflight experience bone loss. After space missions, an interrelation exists between iron stores and bone mineral density (BMD). Bone loss in mice due to unloading is linked to iron excess and involves hepcidin. The potential role of hepcidin in unloading-induced bone loss remains unclear.

Methods Our study conducted relevant experiments using hepcidin knockout mice and their primary osteoblasts as the research subjects. We used the hindlimb unloading (HLU) model and the random positioning machine (RPM) system to simulate weightlessness in vivo and in vitro.

Results HLU mice exhibited reduced hepcidin levels in the serum and liver. Hepcidin knockout further diminished BMD and bone mineral content (BMC) in the femurs of HLU mice. Similarly, the bone volume fraction (BV/TV) and connectivity density (Conn.Dn) followed this downward trend, whereas trabecular separation (Tb.Sp) showed an inverse pattern. Moreover, hepcidin knockout decreased the ultimate load and elastic modulus in the tibias of HLU mice. Hepcidin knockout decreased PINP levels in the serum, a commonly used marker for bone formation, alongside elevated iron levels in the serum, liver, and bone of HLU mice. We also found higher serum MDA and SOD levels in these mice. In vitro, experimental data indicated that hepcidin knockout suppresses the osteoblastic differentiation capacity under RPM conditions. Additionally, this condition upregulates SOST protein levels and downregulates LRP6 and β-catenin protein levels in osteoblasts.

Conclusion Hepcidin knockout exacerbates bone loss in HLU mice, most likely due to reduced osteoblastic activity.

Keywords Hindlimb unloading, Bone loss, Hepcidin, Osteoblast, Wnt/β-catenin signaling pathway, Random positioning machine

*Correspondence:
Peng Shang
shangpeng@nwpu.edu.cn

Full list of author information is available at the end of the article

Introduction

Iron, a critical component in the human body, is essential for oxygen metabolism, energy production, and the maintenance of DNA integrity [1–3]. However, iron excess can be toxic and potentially irreversible damage to tissues and organs, including bone [4]. Osteoporosis is a condition with fragile bones, heightening the likelihood of fractures. Data from clinical studies indicate that osteoporosis is linked to iron overload in conditions like hereditary hemochromatosis, β-thalassemia, and menopause [5–7]. Iron overload is a condition of iron accumulation in the body's multiple organs. Furthermore, iron overload negatively impacts the bone remodeling process, which is crucial for maintaining skeletal health and involves osteoblasts (bone formation cells) that build bone and osteoclasts (bone resorption cells) that break it down [8, 9]. Iron overload suppresses the function of osteoblasts and enhances the activity of osteoclasts [10, 11]. This imbalance is mainly linked to the increased generation of reactive oxygen species (ROS), metabolites of molecular oxygen [10, 11].

Hepcidin, the central iron-regulatory hormone produced by the liver, maintains the body's iron balance by binding to its receptor, ferroportin (FPN) [12, 13]. FPN's function is to transport iron from duodenal enterocytes (the absorption site of dietary iron) and facilitate the release of iron from macrophages and hepatocytes [12, 13]. Upon interaction with FPN, hepcidin triggers its degradation, thus suppressing the release of iron from cells. Postmenopausal women with osteoporosis exhibit lower levels of hepcidin in their blood [14]. In mice, insufficient hepcidin is linked to iron accumulation and bone loss [15, 16]. During spaceflight, bone loss is a critical health issue, which occurs when the rate of bone resorption surpasses that of bone formation [17]. Observations from space missions have indicated an elevation in astronauts' ferritin levels, a key indicator for assessing the body's iron levels [18]. Animal studies have demonstrated that bone loss due to unloading is linked to iron overload, with hepcidin playing a regulatory role in this process [19]. However, the exact function of hepcidin in this process remains unclear.

Materials and methods

Animals procedures

Male mice (eight weeks old), including wild type (WT) and hepcidin knockout ($Hamp^{-/-}$) with C57BL/6J background were originally obtained from Soochow University. We utilized a standard diet to feed the mice. They were kept in an animal room with 12 h of light and 12 h of darkness. The room temperature is 24 ± 2 °C and relative humidity is adjusted to 45–50%. One week prior to the experiment, the mice were acclimated to tail cages to familiarize them with the new environment. All procedures adhered to the guidelines set by the Institutional (Animal Care and Use Committee). Random grouping: (1) $Hamp^{+/+}$-control (wild type mice housed in normal condition for 28 days), (2) $Hamp^{+/+}$-HLU (wild type mice maintained under hindlimb unloading condition for 28 days), (3) $Hamp^{-/-}$-control (hepcidin knockout mice housed in normal condition for 28 days), (4) $Hamp^{-/-}$-HLU (hepcidin knockout mice maintained under hindlimb unloading condition for 28 days).

Simulated weightlessness using hindlimb unloading technology

To reduce mechanical loading on the hindlimbs, the $Hamp^{+/+}$-HLU group and the $Hamp^{-/-}$-HLU group mice were maintained under hindlimb unloading conditions for 28 days. We refer to the methods set by Morey Holton and Globus [20]. The operation steps are as follows: We applied medical tape to wrap around the tail and then fixed it to a copper wire ring. Then, we attached the copper wire ring to a pulley on an overhead bar. The hindlimbs of mice were elevated to maintain a 30° head-down tilt, while the forelimbs remained physiologically loaded. The mice can move and obtain food freely. The control and the $Hamp^{-/-}$ groups were kept under identical conditions but without the tail suspension equipment.

Simulated weightlessness using a random positioning machine

We utilized the RPM system to simulate weightlessness in vitro. The device is composed of two rotating frames (the inner frame and the outer frame), which can be rotated at random speed and direction, and controlled using special software. RPM rotates at random speeds, ensuring that the average gravity vector reliably converges to zero over time. The samples were fixed in the inner frame. We put the RPM system into an ordinary incubator. The control and $Hamp^{-/-}$ groups were placed into the same incubator. Random grouping: (1) $Hamp^{+/+}$-control (cultivation of primary osteoblasts derived from WT mice under normal conditions), (2) $Hamp^{+/+}$-RPM (cultivation of primary osteoblasts derived from WT mice in random positioning machine), (3) $Hamp^{-/-}$-control (cultivation of primary osteoblasts derived from $Hamp^{-/-}$ mice under normal conditions), (4) $Hamp^{-/-}$-RPM (cultivation of primary osteoblasts derived from $Hamp^{-/-}$ mice in random positioning machine).

Tissue collection and sample Ppreparation

Before euthanasia, the mice were anesthetized to ensure they were in a painless and unconscious state. The anesthetic used was pentobarbital sodium, administered at a dosage of 50 mg/kg via intraperitoneal injection. Subsequently, under anesthesia, we used cardiac puncture technology to obtain the mice's blood samples, followed

by euthanasia of the mice through cervical dislocation. Finally, we collected the tissues of the mice and proceeded with processing and preservation.

BMD and BMC measurement

On the 28th day of the experiment, pentobarbital sodium was intraperitoneally injected to anesthetize the mice, and then they were placed under a dual-energy X-ray. The femurs were scanned using the bone density instrument. Then, the instrument's built-in software is used to analyze the femur's BMD and BMC.

Analysis of the femurs using μCT

We used the μCT SkyScan-1176 model manufactured by Bruker to perform the analysis of three-dimensional images of the femurs of the experimental animals. Then, using NRecon, a specialized computer software, we transformed these complex data into three-dimensional visual models. To ensure the reliability of the results, we determined key parameters during the μCT scanning process. The trabecular bone region of interest (ROI) was the interval of 0.5–1.5 millimetres after the disappearance of the distal femoral growth plate. We applied the CTAn tool to study the characteristics of the sample data. To define the range of these features, we set the grayscale threshold to 80. Our observations focused on many key parameters, such as BV/TV (unit: %) and Conn.Dn (unit: $1/mm^3$). At the same time, we also calculated Tb.Sp (unit: mm). The cortical bone region of interest is located 5–6 millimetres beyond the distal femoral growth plate. We used a standard set of grey levels, whose limit is 105. Based on this, we examined some key data to measure the condition of the cortical bone, these parameters include Tt.Ar (unit: mm^2), Ct.Ar (unit: mm^2), and Ct.Th (unit: mm). Their full English names are total area, cortical area, and cortical thickness.

Biomechanical analysis

We applied a three-point bending test to assess the biomechanical characteristics of the tibias. We have chosen a loading speed of one millimetre per minute. After breaking the tibia, the machine will continue to work for two millimetres before stopping. Data were automatically recorded in the computer matched to the machine and generated a load-displacement curve. We used the Matlab analysis platform to provide an in-depth analysis of the key biomechanical properties of the tibia.

Histological evaluation

We used a semi-automated rotary microtome to cut femur and liver samples into 5 μm thick after paraffin embedding. To observe iron deposition status, the slides were selected to be subject to Prussian blue supplemented by the intensification with 3,3'-diaminobenzidine (DAB). The staining principle is that ferric iron in tissues can form a blue ferric ferrocyanide precipitate with ferrocyanides. DAB is added and it undergoes a redox reaction with precipitated ferric iron to form brown compounds, enhancing the specificity of detection.

Iron detection

The samples were placed in a designated container and subjected to a four-hour baking process at 120 °C to remove moisture. Then let it cool naturally to room temperature, weigh it, and record the results in detail. We will then put these dehydrated samples in a high-temperature environment, namely a resistance oven, for six hours of high-temperature treatment. In the same way, after it has cooled to room temperature, measure its weight again and record the result. The last step is to remove the samples that have completed the above two steps from the original container and put them in a 1.5 mL centrifuge tube. We added 300 μl of concentrated nitric acid solution into each centrifuge tube and treated them at 70 °C for two hours. Finally, we utilized atomic absorption spectroscopy to detect the iron content of the samples.

Assessment of biochemical markers

We tested the mice serum levels of PINP (aminoterminal propeptide of type I procollagen), Trap-5b (tartrate-resistant acid phosphatase 5b), and hepcidin using mouse-specific ELISA kits (Gene Beauty Biotechnology Co., Ltd, China). The specific steps were performed as per the manufacturer's guidelines.

Immunoblotting

First, we need to remove the samples from – 80 °C. Then add RIPA into the samples to obtain the total protein. The protein concentration is then measured. Next, we put the mixture containing about thirty micrograms of protein on an SDS-PAGE gel electrophoresis machine for further analysis. Once this step is complete, the proteins need to be transferred to a membrane called PVDF, and then they are exposed to 5% ambient skimmed milk for two hours. The last step is to wash the membrane and soak it at 4 °C with the appropriate antibodies overnight. Then replace it with the secondary antibody and incubate it in a shaker for two hours. Finally, we washed the membranes and collected the images using a chemiluminescence instrument.

Serum oxidative stress indexes evaluation

Before testing, serum samples were removed from the frozen state, and thawed on ice. We used the histochemical reaction method to evaluate the levels of serum oxidative stress indicators (MDA and SOD). The specific steps of the operation are carried out according to the

instructions in the kits. MDA stands for malondialdehyde; SOD denotes superoxide dismutase.

Primary osteoblasts extraction and culture

We obtained primary osteoblasts from the calvaria of neonatal (3–5 days) wild type and hepcidin knockout mice. Then, we washed isolated calvaria three times with a precooled medium and added it to a collagenase and trypsin mixture. After digesting at 37℃ for 4 min, centrifuging and discarding the supernatant. We added precipitate to the collagenase and trypsin mixture, digested at 37℃ for 20 min, and collected primary osteoblasts using centrifugation for 10 min. Repeat digestion and centrifugation of the precipitate twice. Then wash twice with PBS and subculture with normal complete osteoblast medium.

Determination of osteoblastic differentiation

Inoculate cells at an appropriate density in an 18 mm dish. When the cell density is suitable, replace the conventional culture medium with an osteogenic differentiation culture medium and incubate continuously in RPM for 7 days. We employed ALP and alizarin red S (ARS) staining techniques to assess ALP activity and the formation of mineralized nodules. We observed and photographed staining results using a stereomicroscope, and analyzed the stained area using the ImageJ tool. We utilized immunoblotting to measure the protein expression associated with osteogenic differentiation.

Data analysis

Mean ± standard deviation (SD) was applied to present the experimental results. We utilized GraphPad Prism 8.0 to perform statistical analysis and graph plotting. When there were two groups, we utilized an unpaired t-test. When comparing multiple groups, we used a two-way ANOVA, with subsequent application of Tukey's multiple comparison post hoc test. A P-value below 0.05 was considered statistically significant.

Results

Assessment of mice's hepcidin levels

We assessed the serum and liver hepcidin levels of the mice through an ELISA kit and Western blot analysis, respectively. We found that the HLU group had lower hepcidin levels in the serum and liver than the control group (Fig. 1).

The separate and joint effects of hepcidin status and hindlimb unloading on BMD and BMC

We employed DXA scanning technology to evaluate the BMD and BMC values in the femurs of the experimental animals. The DXA data indicated that HLU reduced the femoral BMD and BMC in both genotypes of mice (Fig. 2). Moreover, $Hamp^{-/-}$ mice had lower femoral BMD and BMC than $Hamp^{+/+}$ mice (Fig. 2). There was no interaction between hepcidin status and hindlimb unloading.

The separate and joint effects of hepcidin status and hindlimb unloading on bone microarchitecture

Figure 3A showcased 3D reconstructed visuals of the femoral trabecular bone. In both genotypes of mice, HLU induced reductions in bone volume fraction and connectivity density but increases in trabecular separation (Fig. 3C). Compared to $Hamp^{+/+}$ mice, $Hamp^{-/-}$ mice had lower bone volume fraction and connectivity density and higher trabecular separation (Fig. 3C). No interaction between hepcidin status and hindlimb unloading was observed.

Figure 3B displayed 3D reconstruction graphics of the femoral cortical bone. The results showed that HLU decreased cortical thickness and cortical area and did not change total area (Fig. 3D). $Hamp^{-/-}$ reduced cortical thickness in control mice, $Hamp^{-/-}$ did not affect cortical area and total area across control and HLU mice (Fig. 3D). There was no interaction between hepcidin status and hindlimb unloading.

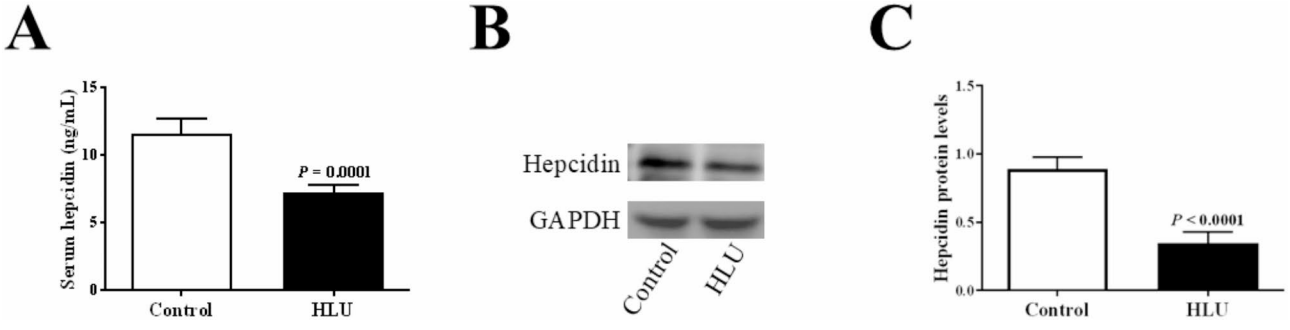

Fig. 1 Hepcidin levels in each group were evaluated. (**A**) Presents serum hepcidin concentrations. (**B**) Image acquisition of hepcidin protein in the liver. (**C**) Grayscale analysis of hepatic hepcidin protein. ($n = 4–5$ per group)

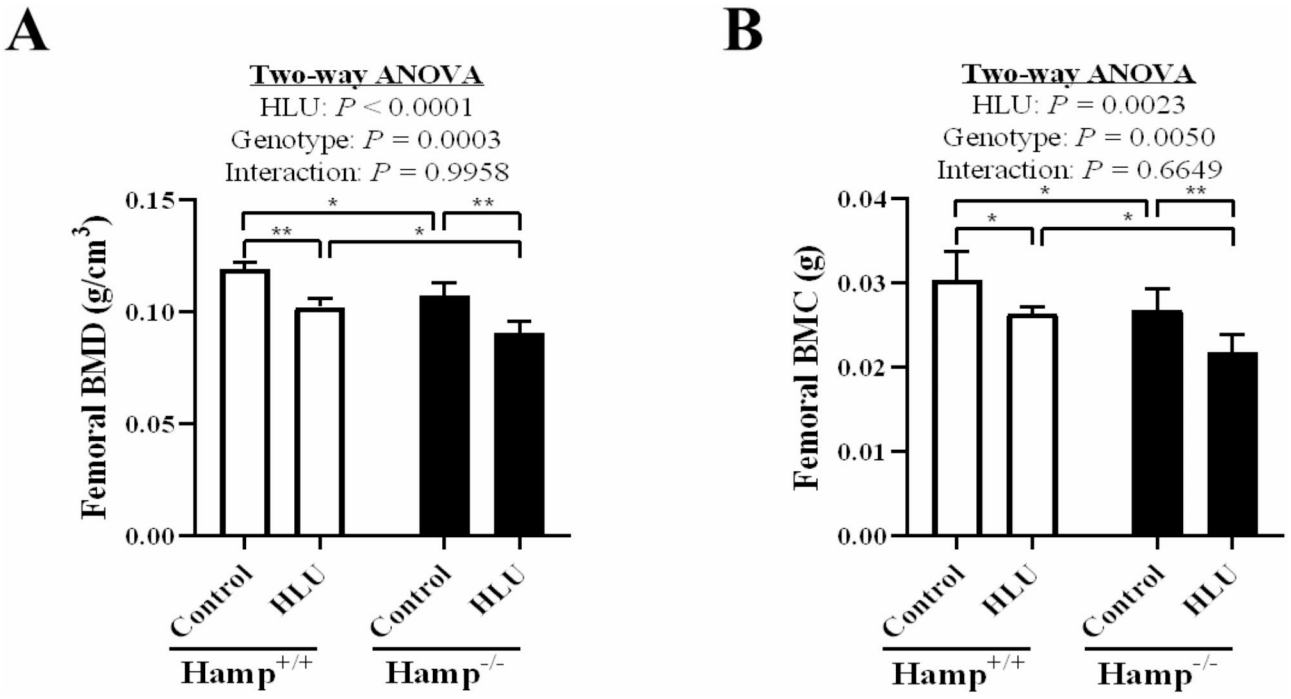

Fig. 2 Statistical charts of BMD and BMC. BMD (**A**) and BMC (**B**) in the femurs were displayed. ($n = 4$–5 per group; $P < 0.05$ is considered statistically significant; * represents $P < 0.05$ and ** denotes $P < 0.01$)

The separate and joint effects of hepcidin status and hindlimb unloading on biomechanical properties

In HLU mice, tibial biomechanical properties including ultimate load, ultimate stress, elastic modulus, and stiffness were reduced relative to control mice (Fig. 4). $Hamp^{-/-}$ mice had lower ultimate load and elastic modulus but unaffected ultimate stress and stiffness than $Hamp^{+/+}$ mice (Fig. 4). There was no interaction between hepcidin status and hindlimb unloading (Fig. 4).

The separate and joint effects of hepcidin status and hindlimb unloading on serum PINP and Trap-5b levels

HLU reduced serum PINP levels and increased serum Trap-5b levels in both genotypes of mice (Fig. 5). $Hamp^{-/-}$ decreased serum PINP levels across control and HLU mice, $Hamp^{-/-}$ elevated serum Trap-5b levels in control mice (Fig. 5). No significant interaction was noted between hepcidin status and hindlimb unloading.

The separate and joint effects of hepcidin status and hindlimb unloading on iron levels

Perls DAB-enhanced iron staining data showed that HLU increased iron levels in the liver and bone in both genotypes of mice (Fig. 6A and B). Compared to $Hamp^{+/+}$ mice, $Hamp^{-/-}$ mice exhibited elevated iron levels in the liver and bone (Fig. 6A and B). Moreover, we determined iron levels in the serum, liver, and bone using atomic absorption technology. The outcomes indicated that HLU raised serum, liver, and bone iron contents across $Hamp^{+/+}$ and $Hamp^{-/-}$ mice (Fig. 6C, D, and E). $Hamp^{-/-}$ mice had higher serum, liver, and bone iron contents than $Hamp^{+/+}$ mice (Fig. 6C, D, and E). There was no interaction between hepcidin status and hindlimb unloading.

The separate and joint effects of hepcidin status and hindlimb unloading on oxidative stress markers

The statistical data showed that HLU increased serum MDA and SOD levels in $Hamp^{-/-}$ mice (Fig. 7). $Hamp^{-/-}$ elevated serum MDA and SOD levels in control and HLU mice (Fig. 7). There is a significant interaction between hepcidin status and hindlimb unloading on serum MDA levels.

The separate and joint effects of hepcidin status and random positioning machine on osteoblastic differentiation capacity

RPM inhibited the ALP activity and mineralization capacity of primary osteoblasts derived from both genotypes of mice (Fig. 8). Compared to primary osteoblasts derived from $Hamp^{+/+}$ mice, those from $Hamp^{-/-}$ mice exhibited lower ALP activity and mineralization capacity (Fig. 8). There was no interaction between hepcidin status and random positioning machine (Fig. 8).

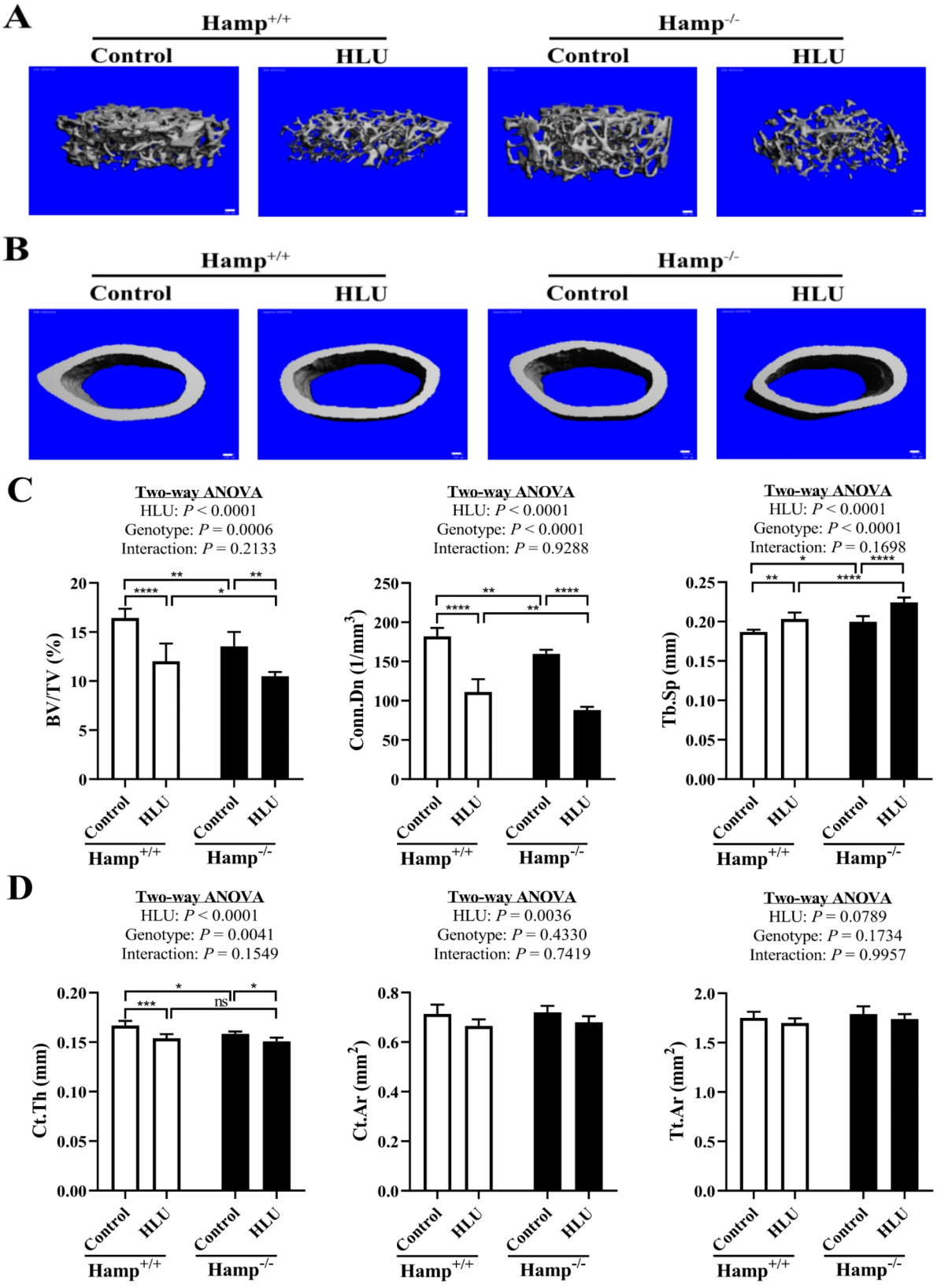

Fig. 3 μCT results. (**A**) 3D reconstruction images of femoral trabecular bone. (**B**) Crucial microstructural parameters of trabecular bone. (**C**) 3D reconstructed visuals of femoral cortical bone. (**D**) Key architectural features of cortical bone. bar = 100 μm. ($n = 4$–6 per group; $P < 0.05$ is considered statistically significant; * represents $P < 0.05$, *** indicates $P < 0.001$, and ns denotes no significant)

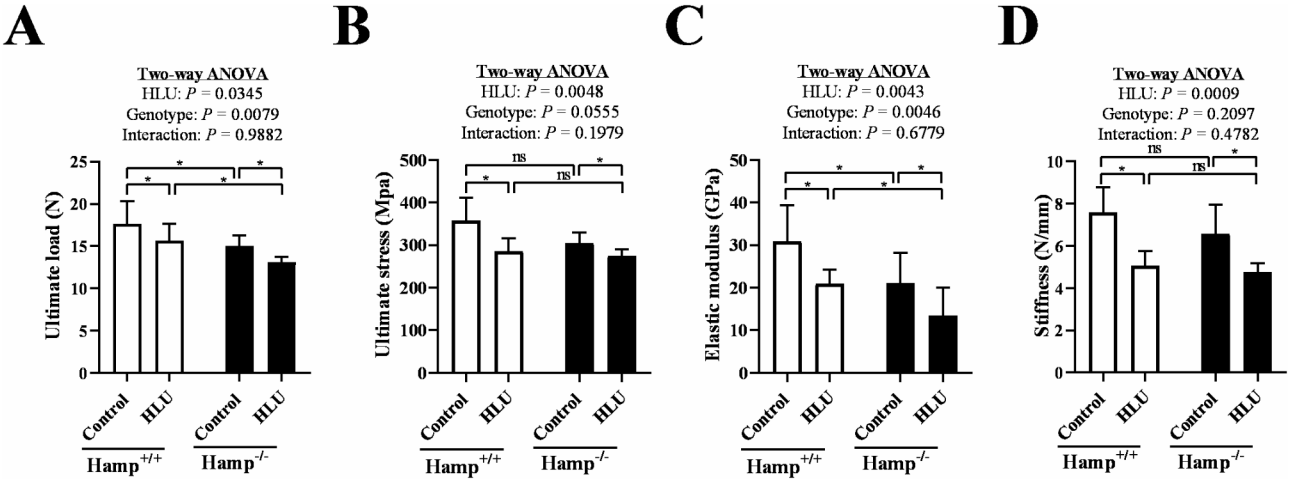

Fig. 4 Displays the tibial biomechanical properties. (**A**-**D**) The key biomechanical indexes. ($n = 4$–6 per group; $P < 0.05$ is considered statistically significant; * represents $P < 0.05$ and ns denotes no significant)

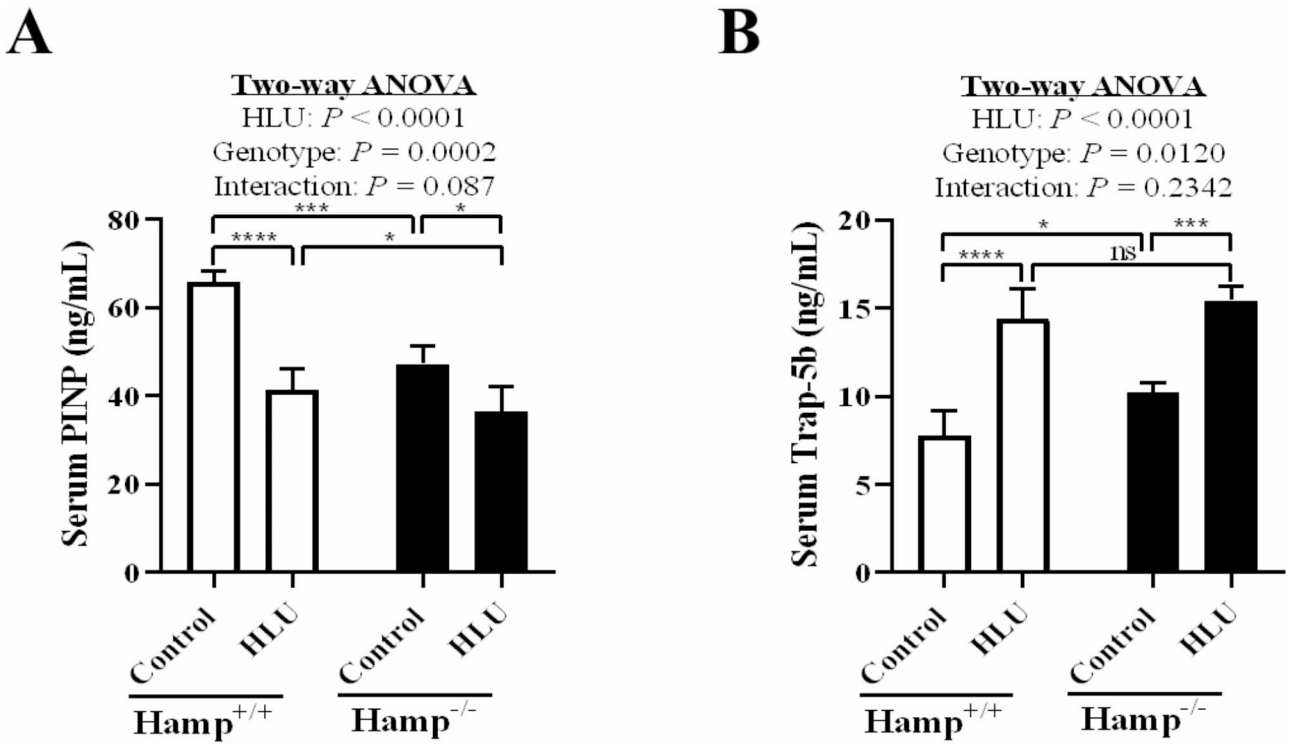

Fig. 5 Analysis of bone remodeling parameters. (**A**) Statistical figure of serum PINP levels. (**B**) Displays the graph of serum Trap-5b levels. ($n = 4$–6 per group; $P < 0.05$ is considered statistically significant; * represents $P < 0.05$, *** indicates $P < 0.001$, **** signifies $P < 0.0001$ and ns denotes no significant)

The separate and joint effects of hepcidin status and random positioning machine on expression of proteins in osteoblasts

Sclerostin (encoded by SOST) acts as a suppressor of the Wnt pathway. It hinders the canonical Wnt pathway by attaching to LRP5/6 receptors. RPM downregulated LRP6, β-catenin, and Runx2 protein levels and upregulated SOST protein levels of primary osteoblasts in both genotypes (Fig. 9). $Hamp^{-/-}$ repressed LRP6 and β-catenin protein levels in primary osteoblasts across control and RPM groups, $Hamp^{-/-}$ suppressed Runx2 protein levels in primary osteoblasts of control mice (Fig. 9). There was no interaction between hepcidin status and random positioning machine.

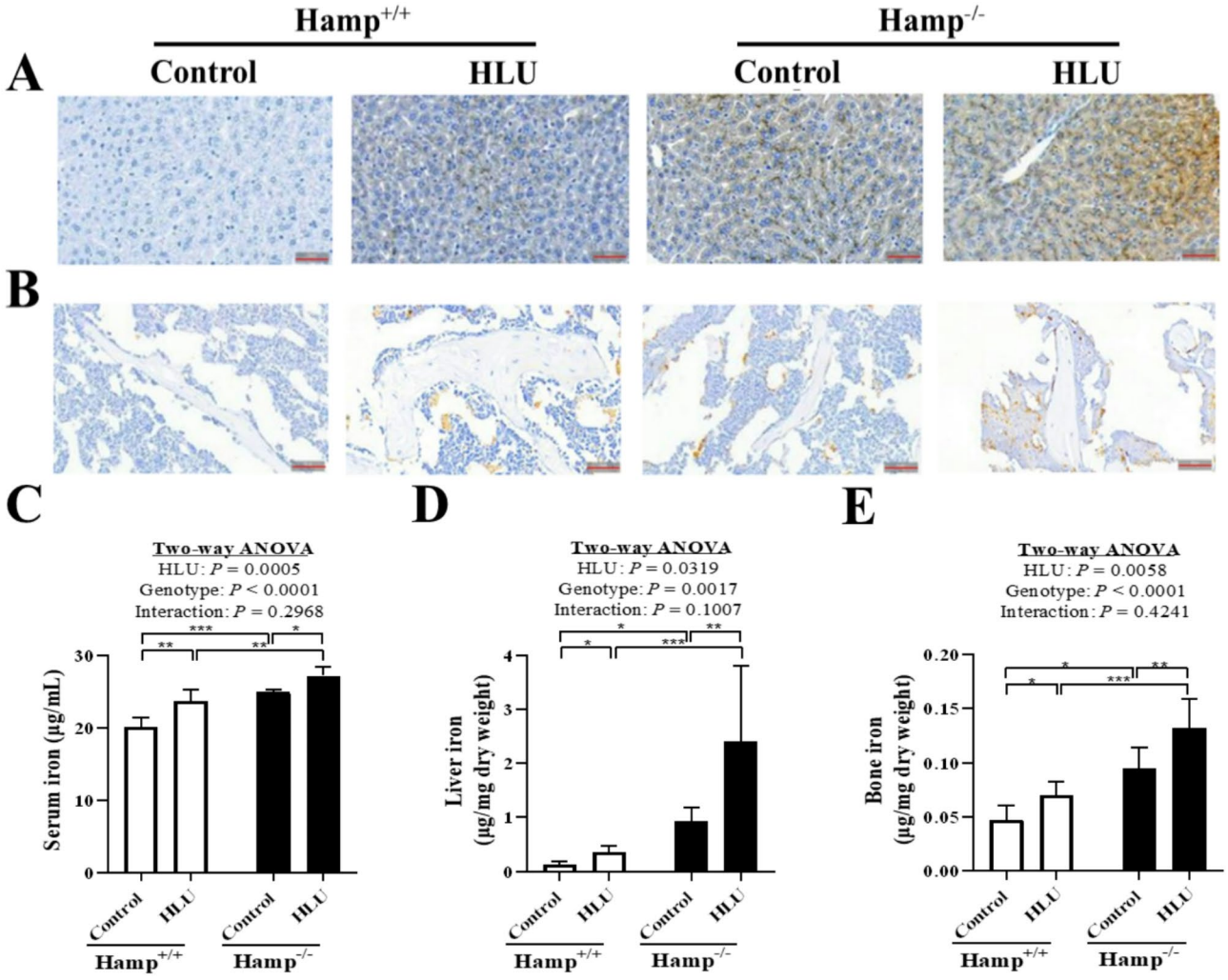

Fig. 6 Liver, bone, and serum iron levels in each group. (**A** and **B**) Iron staining results, bar = 50 μm. (**C**-**E**) The results of atomic absorption spectrometry. ($n = 4$–6 per group; $P < 0.05$ is considered statistically significant; * represents $P < 0.05$, ** indicates $P < 0.01$, and *** signifies $P < 0.001$)

Discussion

In space travel, the principal driver of bone loss due to weightlessness (the lack of gravity) is the absence of mechanical loading [21]. Hepcidin is an oligopeptide responsible for regulating the body's iron homeostasis. Insufficient hepcidin leads to iron overload, while its excess results in iron insufficiency. Unloading alone and hepcidin insufficiency alone result in bone defects [15, 16, 22]. Moreover, iron overload has been identified as a significant contributor to bone loss, including unloading-induced bone loss. There is a scarcity of studies examining the influence of hepcidin on bone health under weightlessness conditions. Due to the rare opportunity and high cost of space travel, many known pathologies of bone loss in weightlessness conditions are derived from terrestrial simulation models [23–25]. So, we used the hindlimb unloading mouse model to simulate weightlessness in vivo. Initially, we evaluated the hepcidin levels in the mice. The findings revealed that HLU mice exhibited reduced hepcidin levels, contrary to the report by Zi Xu [19]. This discrepancy may be attributed to the HLU-induced decline in Nrf2 expression in the liver, subsequently leading to reduced BMP6 and hepcidin expression [26, 27].

Hamp$^{-/-}$ reduced the BMD and BMC values and impacted the trabecular microstructure, consistent with previous reports [16, 28]. Hamp$^{-/-}$ exerted minimal effects on the cortical microstructure. The possible reason is that cortical bone possesses a compact structure and is relatively less sensitive to hepcidin deficiency. From the perspective of biomechanical characteristics, ultimate load and elastic modulus were reduced by Hamp$^{-/-}$, similar to the reported literature [15]. HLU decreased the BMD and BMC and injured the trabecular microstructure, consistent with our previous report [22]. HLU had little effect on the cortical microstructure, similar to our previously reported literature [22]. HLU diminished all the biomechanical parameters, aligning with the

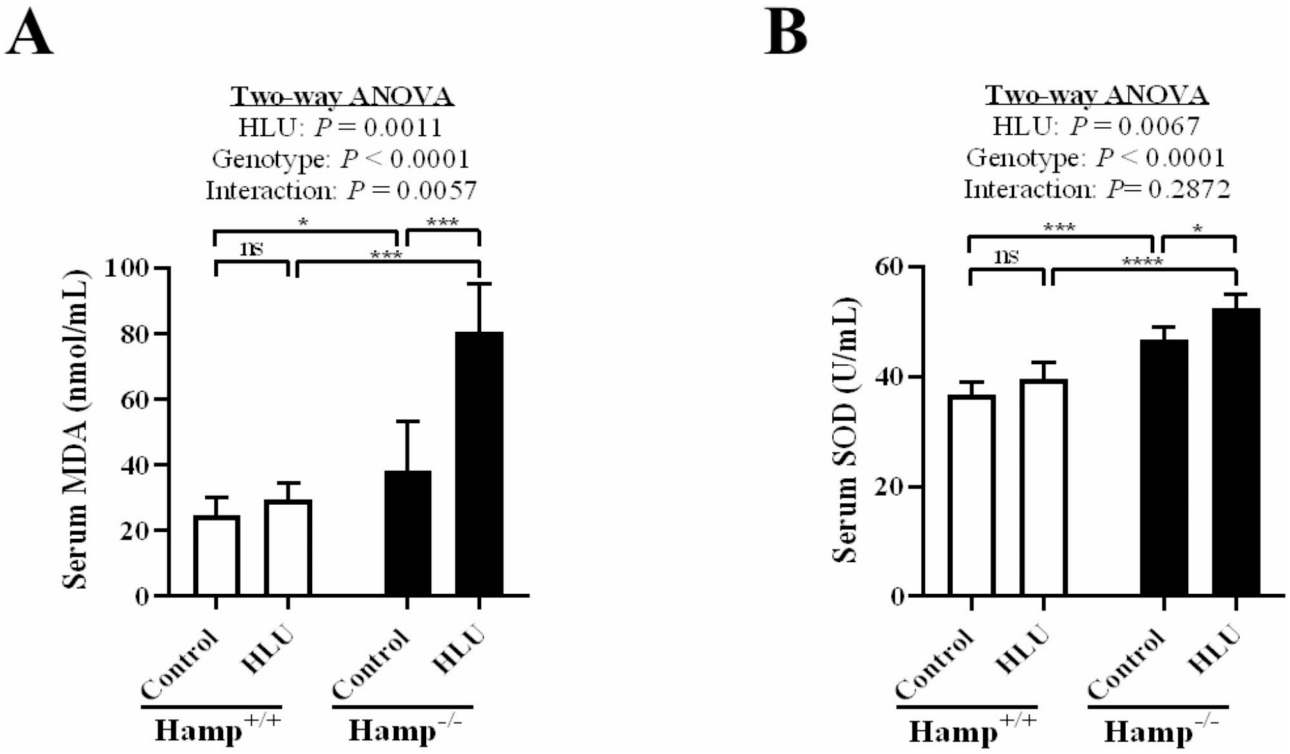

Fig. 7 Displays oxidative stress indicators. Serum MDA (**A**) and SOD (**B**). ($n = 4$–6 per group; $P < 0.05$ is considered statistically significant; * represents $P < 0.05$, *** indicates $P < 0.001$, **** signifies $P < 0.0001$, and ns denotes no significant)

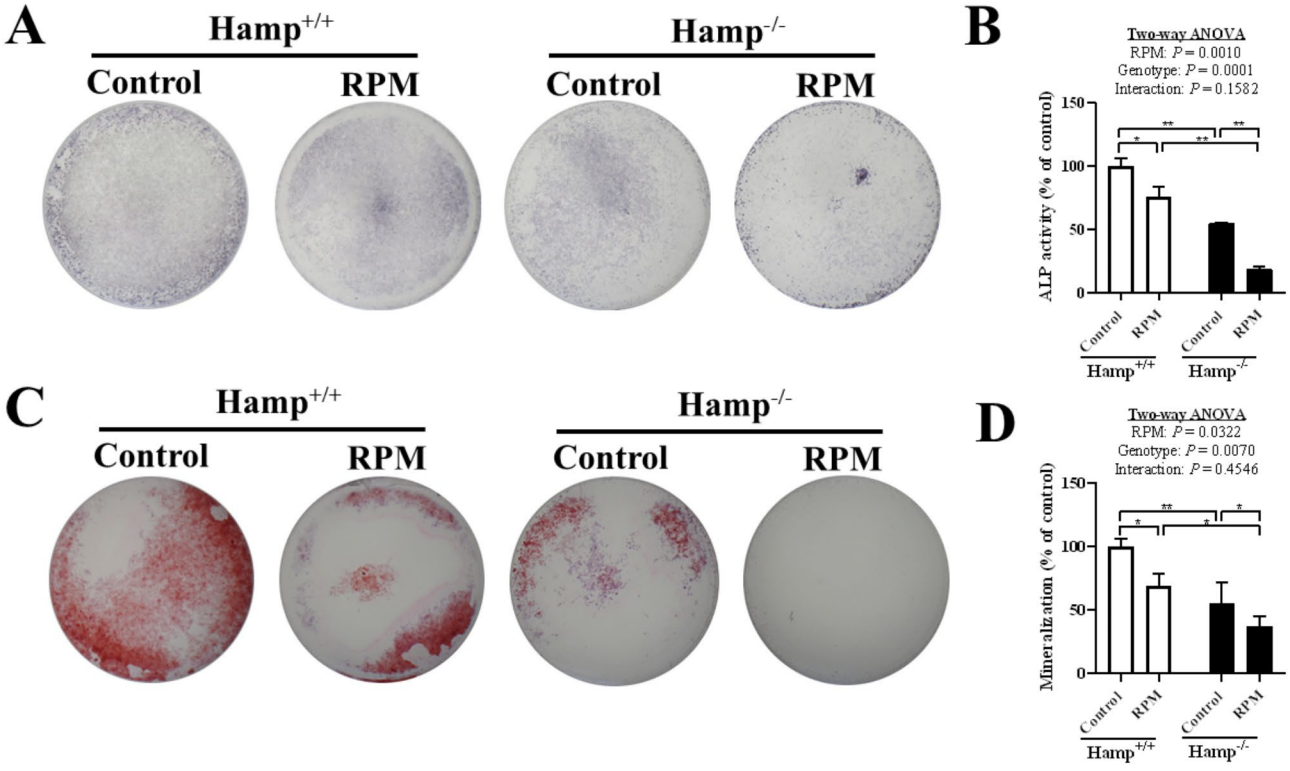

Fig. 8 Primary osteoblastic ALP activity and mineralization capacity. (**A**) Primary osteoblasts were stained using an Alkaline Phosphatase Assay Kit. (**B**) ALP staining results were analyzed. (**C**) Mineralized nodule of primary osteoblasts was stained. (**D**) The nodule area was evaluated. ($n = 3$; $P < 0.05$ is considered statistically significant; * represents $P < 0.05$ and ** denotes $P < 0.01$)

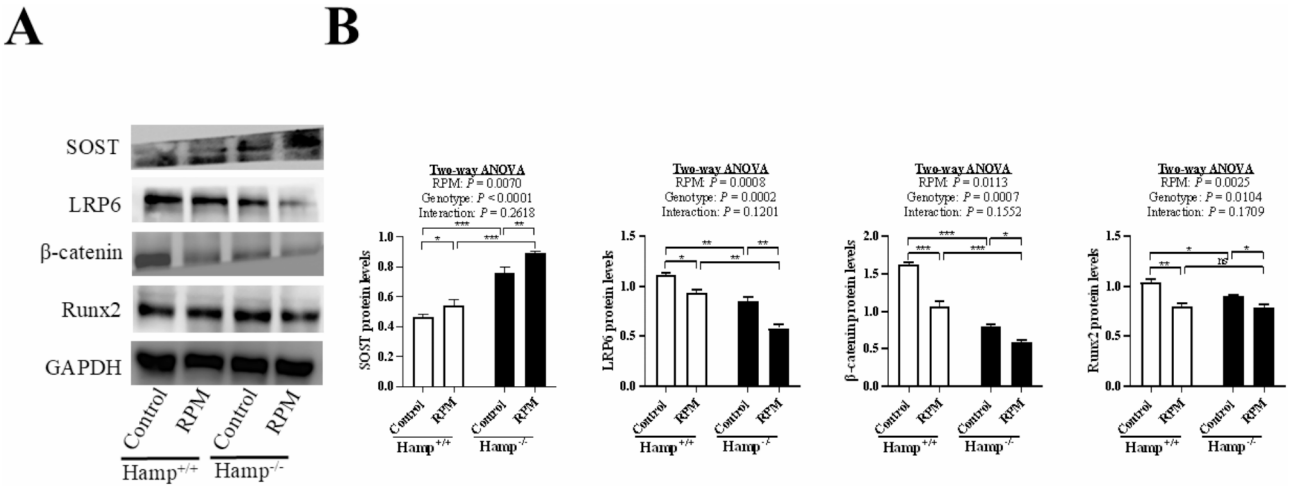

Fig. 9 Immunoblotting results. (**A**) Image acquisition of proteins. (**B**) Statistical analysis of proteins. ($n = 3$; $P < 0.05$ is considered statistically significant; * represents $P < 0.05$, ** denotes $P < 0.01$, *** indicates $P < 0.001$, and ns displays no significant)

earlier findings [22, 29]. The above results indicated that hepcidin knockout exacerbates bone loss in mice caused by unloading, due to its independent role.

Next, we evaluated the indicators of bone formation and bone resorption. The results showed that HLU inhibited bone formation and promoted bone resorption. Hamp$^{-/-}$ suppressed bone formation in control and HLU mice, and Hamp$^{-/-}$ enhanced bone resorption in control mice. The bone resorption across Hamp$^{+/+}$-HLU and Hamp$^{-/-}$-HLU groups is similar. It's likely because hindlimb unloading has a more significant impact on bone resorption. Unloading removes the mechanical loads of bones, which directly affects osteoclastic activity [30]. In contrast, although hepcidin deficiency also affects bone resorption, its effect may be relatively weak and insufficient to produce significant cumulative effects under the dominant role of hindlimb unloading. Another possibility is that the impact of hepcidin status on bone resorption is controlled by other unidentified factors that were not accounted for in the study design. The main reason for the inhibition of bone formation by HLU and Hamp$^{-/-}$ may be the decreased differentiation ability of osteoblasts, which can be confirmed by in vitro experiments. The Wnt/β-catenin pathway plays a vital role in osteoblastic differentiation. We found that RPM inhibited the Wnt/β-catenin signaling pathway. Hamp$^{-/-}$ also repressed the Wnt/β-catenin pathway. These findings demonstrated that hepcidin knockout exacerbates bone loss caused by unloading, most likely due to reduced osteoblastic activity through inhibiting the Wnt/β-catenin pathway.

Iron plays an important role in bone remodelling. So, we further assessed the iron levels in the body. Iron staining and iron content detection data indicated that HLU increased the iron levels in the body, consistent with a previous report [19]. Hamp$^{-/-}$ raised the iron levels in the body, similar to the reported literature [28]. Oxidative stress is "an imbalance between the production of ROS and antioxidants, resulting in damage to cells" [31]. Through the Fenton reaction, excessive iron facilitates the production of a large amount of ROS. Evidence from an animal experiment illustrated that iron overload-induced bone loss is linked to oxidative stress [32]. Therefore, we evaluated the oxidative stress markers in the mice. MDA is one of the final products of lipid peroxidation in living organisms, which is the decomposition product of polyunsaturated fatty acids under the attack of ROS [33]. The antioxidant SOD is a widely present antioxidant enzyme in living organisms [34]. Hamp$^{-/-}$ elevated serum MDA and SOD levels across control and HLU mice. HLU increased serum MDA and SOD levels in Hamp$^{-/-}$ mice. The increased level of serum MDA in Hamp$^{-/-}$-HLU mice is much greater than that of SOD, indicating that SOD can only partially eliminate the production of MDA, thereby leading to oxidative stress.

There was a significant interaction between hepcidin status and hindlimb unloading on serum MDA levels. The possible reason is that hepcidin deficiency leads to iron overload, subsequently triggering oxidative stress [35]. HLU further exacerbated the levels of iron in Hamp$^{-/-}$ mice. Thereby, exacerbating oxidative stress levels, resulting in a significant increase in serum MDA levels. However, no interaction between hepcidin status and hindlimb unloading was noted on bone parameters. This may be because these two factors influence oxidative stress and bone health via distinct biochemical mechanisms. Specifically, hindlimb unloading may lead to reduced mechanical loading on the bones, resulting in an imbalance in bone remodelling and subsequent bone loss. In this case, hepcidin deficiency might further exacerbate the bone loss process. On the one hand, hepcidin deficiency may lead to iron overload and increase

oxidative stress, resulting in accelerated bone loss. On the other hand, iron overload may directly affect the activity and function of osteoblasts and osteoclasts, leading to accelerated bone loss. Moreover, whether the interaction between hepcidin status and hindlimb unloading on oxidative stress, leads to their interaction on bone parameters. Bone parameters of the lumbar spine and tibia should be evaluated.

The following are the constraints of this research. Firstly, the number of subjects in each animal group ($n = 4–6$) is limited. Due to the limited sample size, some measurements with biological significance did not yield statistically significant results. Secondly, the depth of mechanism exploration is insufficient. While our findings suggest that hepcidin knockout intensifies the suppressive impact of RPM on osteogenic differentiation and alters the expression of Wnt/β-catenin signaling pathway-related proteins, further validation is needed. Future studies should employ inhibitors of the Wnt/β-catenin pathway in vitro to confirm these observations. Thirdly, it is still uncertain whether hepcidin knockout also intensifies the suppressive impact of RPM on osteogenic differentiation through other signaling pathways. Fourthly, it is essential to investigate the effects of the Wnt/β-catenin signaling pathway on bone defect in hepcidin knockout mice subjected to HLU through in vivo studies. Fifthly, there is a lack of validation experiments for oxidative stress. At the animal level, it needs to identify whether oxidative stress is involved in the exacerbation of bone loss in HLU mice following hepcidin knockout. Lastly, a lack of osteoclast-related experiments is also a limitation of this study. We should identify the effects of hepcidin knockout on osteoclastic differentiation in primary bone marrow macrophages under RPM conditions.

Conclusion

In summary, the results indicated that hepcidin knockout exacerbates bone loss in mice in response to hindlimb unloading, most likely due to reduced osteoblastic activity. Mechanistically, hepcidin knockout may reduce osteoblastic activity by affecting the Wnt/β-catenin signaling pathway.

Supplementary Information

The online version contains supplementary material available at https://doi.org/10.1186/s12891-025-08515-0.

Supplementary Material 1

Supplementary Material 2

Acknowledgements
We would love to express utmost respect to all the authors of the articles cited in this article.

Author contributions
Research planning: PS and XC; Experimental subjects: YX; Experiment execution: XC, JW, CZ, and GZ; Data gathering: XC and JW; Data interpretation: XC and ZY; Manuscript composition: XC and PS; Final manuscript endorsement: all contributors; XC and PS are responsible for the reliability of the data analysis.

Funding
This research was funded by Shenzhen Basic Research Special Projects (JCYJ20210324141414034), Space Medical Experiment Project of China Manned Space Program (HYZHXM01008), and Space Utilization Project of China Manned Space Program (YYWT-0901-EXP-04).

Data availability
Data is provided within the manuscript or supplementary information files.

Declarations

Ethics approval and consent to participate
The Animal Ethics Committee of Northwestern Polytechnical University approved this research. All experimental operations involving mice were conducted according to the institution's guidelines and regulations. All animal procedures adhered to the Basel Declaration (https://animalresearchtomorrow.org/en) and the ARRIVE guidelines (https://arriveguidelines.org).

Consent for publication
Not applicable.

Competing interests
The authors declare no competing interests.

Author details
[1]School of Life Sciences, Northwestern Polytechnical University, Xi'an 710072, China
[2]Research & Development Institute in Shenzhen, Northwestern Polytechnical University, Shenzhen 518057, China
[3]Key Laboratory for Space Bioscience and Biotechnology, Institute of Special Environmental Biophysics, Northwestern Polytechnical University, Xi'an 710072, China
[4]Department of Orthopaedics, The Second Affiliated Hospital of Soochow University, Suzhou 215004, China

Received: 16 December 2024 / Accepted: 11 March 2025
Published online: 18 March 2025

References

1. Dutt S, Hamza I, Bartnikas TB. Molecular mechanisms of iron and Heme metabolism. Annu Rev Nutr. 2022;42:311–35.
2. Puig S, Ramos-Alonso L, Romero AM, Martínez-Pastor MT. The elemental role of iron in DNA synthesis and repair. Metallomics. 2017;9(11):1483–500.
3. Cilloni D, Ravera S, Calabrese C, Gaidano V, Niscola P, Balleari E, et al. Iron overload alters the energy metabolism in patients with myelodysplastic syndromes: results from the multicenter FISM BIOFER study. Sci Rep. 2020;10(1):9156.
4. Zhang H, Yang F, Cao Z, Xu Y, Wang M. The influence of iron on bone metabolism disorders. Osteoporos Int. 2024;35(2):243–53.
5. Valenti L, Varenna M, Fracanzani AL, Rossi V, Fargion S, Sinigaglia L. Association between iron overload and osteoporosis in patients with hereditary hemochromatosis. Osteoporos Int. 2009;20(4):549–55.
6. Rossi F, Perrotta S, Bellini G, Luongo L, Tortora C, Siniscalco D, et al. Iron overload causes osteoporosis in thalassemia major patients through interaction with transient receptor potential vanilloid type 1 (TRPV1) channels. Haematologica. 2014;99(12):1876–84.
7. Cheng Q, Zhang X, Jiang J, Zhao G, Wang Y, Xu Y et al. Postmenopausal iron overload exacerbated bone loss by promoting the degradation of type I collagen. Biomed Res Int. 2017; 2017:1345193.
8. Jiang ZX, Wang H, Qi GB, Jiang C, Chen KN, Yan ZQ. Iron overload-induced ferroptosis of osteoblasts inhibits osteogenesis and promotes osteoporosis: an in vitro and in vivo study. IUBMB Life. 2022;74(11):1052–69.

9. Wang X, Fei BB, Shen GS, Jiang Y, Zhang W, Huang X. Iron overload increases osteoclastogenesis and aggravates the effects of ovariectomy on bone mass. J Endocrinol. 2015;226(3):121–34.
10. Jia P, Xu YJ, Zhang ZL, Li K, Li B, Zhang W, et al. Ferric ion could facilitate osteoclast differentiation and bone resorption through the production of reactive oxygen species. J Orthop Res. 2012;30(11):1843–52.
11. He YF, Ma Y, Gao C, Zhao GY, Zhang LL, Li GF, et al. Iron overload inhibits osteoblast biological activity through oxidative stress. Biol Trace Elem Res. 2013;152(2):292–6.
12. Nemeth E, Ganz T. Hepcidin-ferroportin interaction controls systemic iron homeostasis. Int J Mol Sci. 2021;22(12):6493.
13. Billesbølle CB, Azumaya CM, Kretsch RC, Powers AS, Gonen S, Schneider S, et al. Structure of hepcidin-bound Ferroportin reveals iron homeostatic mechanisms. Nature. 2020;586(7831):807–11.
14. Zhang H, Wang AF, Shen GS, Wang X, Liu GW, Yang F, et al. Hepcidin-induced reduction in iron content and PGC-1β expression negatively regulates osteoclast differentiation to play a protective role in postmenopausal osteoporosis. Aging. 2021;13(8):11296–314.
15. Sun L, Guo W, Yin C, Zhang S, Qu G, Hou Y, et al. Hepcidin deficiency undermines bone load-bearing capacity through inducing iron overload. Gene. 2014;543(1):161–5.
16. Li GF, Zhang H, Wu JD, Wang AF, Yang F, Chen B, et al. Hepcidin deficiency causes bone loss through interfering with the canonical Wnt/β-catenin pathway via forkhead box O3a. J Orthop Translat. 2020;23:67–76.
17. Carmeliet G, Vico L, Bouillon R. Space flight: a challenge for normal bone homeostasis. Crit Rev Eukaryot Gene Expr. 2001;11(1–3):131–44.
18. Zwart SR, Morgan JL, Smith SM. Iron status and its relations with oxidative damage and bone loss during long-duration space flight on the international space station. Am J Clin Nutr. 2013;98(1):217–23.
19. Xu Z, Sun WJ, Li YH, Ling SK, Zhao CY, Zhong GH, et al. The regulation of iron metabolism by Hepcidin contributes to unloading-induced bone loss. Bone. 2017;94:152–61.
20. Morey-Holton ER, Globus RK. Hindlimb unloading rodent model: technical aspects. J Appl Physiol (1985). 2002;92(4):1367–77.
21. Bikle DD, Halloran BP. The response of bone to unloading. J Bone Min Metab. 1999;17(4):233–44.
22. Yang J, Meng X, Dong D, Xue Y, Chen X, Wang S, et al. Iron overload involved in the enhancement of unloading-induced bone loss by hypomagnetic field. Bone. 2018;114:235–45.
23. Li JH, Geng JY, Lin TT, Cai MX, Sun Y. A mouse model of disuse osteoporosis based on a movable noninvasive 3D-printed unloading device. J Orthop Translat. 2022;33:1–12.
24. Böcker J, Schmitz MT, Mittag U, Jordan J, Rittweger J. Between-subject and within-subject variaton of muscle atrophy and bone loss in response to experimental bed rest. Front Physiol. 2022;12:743876.
25. Guo Q, Chen N, Patel K, Wan M, Zheng J, Cao X. Unloading-induced skeletal interoception alters hypothalamic signaling to promote bone loss and fat metabolism. Adv Sci (Weinh). 2023;10(35):e2305042.
26. Che J, Ren W, Chen X, Wang F, Zhang G, Shang P. PTH 1–34 promoted bone formation by regulating iron metabolism in unloading-induced bone loss. Front Endocrinol (Lausanne). 2023;13:1048818.
27. Pauk M, Grgurevic L, Brkljacic J, Kufner V, Bordukalo-Niksic T, Grabusic K, et al. Exogenous BMP7 corrects plasma iron overload and bone loss in Bmp6$^{-/-}$ mice. Int Orthop. 2015;39(1):161–72.
28. Shen GS, Yang Q, Jian JL, Zhao GY, Liu LL, Wang X, et al. Hepcidin1 knockout mice display defects in bone microarchitecture and changes of bone formation markers. Calcif Tissue Int. 2014;94(6):632–9.
29. Zhang GJ, Zhen CX, Yang JC, Zhang ZY, Wu YD, Che JM, et al. 1–2 T static magnetic field combined with Ferumoxytol prevent unloading-induced bone loss by regulating iron metabolism in osteoclastogenesis. J Orthop Translat. 2022;3:38:126–40.
30. Saxena R, Pan G, Dohm ED, McDonald JM. Modeled microgravity and hindlimb unloading sensitize osteoclast precursors to RANKL-mediated osteoclastogenesis. J Bone Min Metab. 2011;29(1):111–22.
31. van der Pol A, van Gilst WH, Voors AA, van der Meer P. Treating oxidative stress in heart failure: past, present and future. Eur J Heart Fail. 2019;21(4):425–35.
32. Tsay J, Yang ZW, Ross FP, Cunningham-Rundles S, Lin H, Coleman R, et al. Bone loss caused by iron overload in a murine model: importance of oxidative stress. Blood. 2010;116(14):2582–9.
33. Del Rio D, Stewart AJ, Pellegrini N. A review of recent studies on malondialdehyde as toxic molecule and biological marker of oxidative stress. Nutr Metab Cardiovasc Dis. 2005;15(4):316–28.
34. McCord JM, Edeas MA. SOD, oxidative stress and human pathologies: a brief history and a future vision. Biomed Pharmacother. 2005;59(4):139–42.
35. Ma J, Wang A, Zhang H, Liu B, Geng Y, Xu Y, et al. Iron overload induced osteocytes apoptosis and led to bone loss in Hepcidin(-/-) mice through increasing sclerostin and RANKL/OPG. Bone. 2022;164:116511.

Publisher's note